Journal of ELECTRONIC MATERIALS, Vol. 46, No. 9, 2017
DOI: 10.1007/s11664-017-5596-4

Progress of MCT Detector Technology at AIM Towards Smaller Pitch and Lower Dark Current

D. EICH,[1,2] W. SCHIRMACHER,[1] S. HANNA,[1] K.M. MAHLEIN,[1] P. FRIES,[1] and H. FIGGEMEIER[1]

1.—AIM INFRAROT-MODULE GmbH, Theresienstraße 2, 74072 Heilbronn, Germany. 2.—e-mail: detlef.eich@aim-ir.com

We present our latest results on cooled *p*-on-*n* planar mercury cadmium telluride (MCT) photodiode technology. Along with a reduction in dark current for raising the operating temperature (T_{op}), AIM INFRAROT-MODULE GmbH (AIM) has devoted its development efforts to shrinking the pixel size. Both are essential requirements to meet the market demands for reduced size, weight and power and high-operating temperature applications. Detectors based on the *p*-on-*n* technology developed at AIM now span the spectrum from the mid-wavelength infrared (MWIR) to the very long wavelength infrared (VLWIR) with cut-off wavelengths from 5 μm to about 13.5 μm at 80 K. The development of the *p*-on-*n* technology for VLWIR as well as for MWIR is mainly implemented in a planar photodetector design with a 20-μm pixel pitch. For the VLWIR, dark currents significantly reduced as compared to 'Tennant's Rule 07' are demonstrated for operating temperatures between 30 K and 100 K. This allows for the same dark current performance at a 20 K higher operating temperature than with previous AIM technology. For MWIR detectors with a 20-μm pitch, noise equivalent temperature differences of less than 30 mK are obtained up to 170 K. This technology has been transferred to our small pixel pitch high resolution (XGA) MWIR detector with 1024 $\times$ 768 pixels at a 10-μm pitch. Excellent performance at an operating temperature of 160 K is demonstrated.

Key words: AIM, infrared detector, MCT, VLWIR, MWIR, HOT, small pixel pitch

INTRODUCTION

The growing demand for high operating temperature (HOT) infrared (IR) detectors and longer mission time has been one of the key drivers for material and technology improvements of cooled IR detectors in recent years.[1–3] Beside an increase in operating temperature (T_{op}), the reduction in pixel size is happening at the same time to meet the requirements of reduced size, weight and power (SWaP) and higher spatial resolution of up-to-date present as well as future IR focal plane arrays (FPA).[4–6] To achieve these goals, research efforts have been made for almost all known infrared material systems such as HgCdTe (MCT), InSb and III–V superlattices.[7–10]

In the long wavelength infrared (LWIR) and very long wavelength infrared (VLWIR) spectral ranges, an increase in operating temperature is significantly more difficult due to the stringent demands on detector material quality and detector processing connected to the narrow energy band gap of the detector material. With LWIR HOT detector applications expanding, AIM INFRAROT-MODULE GmbH (AIM) as a leader in LWIR MCT detectors has addressed the challenge. During the last 4 years AIM matured the *p*-on-*n* LWIR technology, a key technology for high-performance small pixel pitch planar LWIR HOT MCT devices.[5]

(Received October 24, 2016; accepted May 16, 2017; published online May 30, 2017)

After attaining excellent electro-optical performance results for the VLWIR, AIM has extended the wavelength range and transferred its *p*-on-*n* technology to mid-wavelength infrared (MWIR) MCT photodiodes. Again, as an array format for the development phase, a 640 × 512 pixel, 20-μm pitch design was chosen. The *p*-on-*n* FPA shows comparable performance to AIM's latest HOT GEN2 FPA in standard *n*-on-*p* technology. The performance regarding noise equivalent temperature difference (NETD) and operability shows good results up to 170 K.

IR sensor arrays with a 15-μm pixel pitch constituted the standard pixel size for IR imaging applications in recent years.[2] For the next generation of SWAP detectors, a pixel pitch of 10 μm appears to have emerged as a new standard pixel size.[11] Encouraged by the excellent results for 20-μm pitch diode arrays in the MWIR spectral range, the *p*-on-*n* technology has recently been applied to AIM's new small pixel pitch high resolution (XGA) MWIR detector with 1024 × 768 pixels and a 10-μm pitch.

Here, we present the results of our *p*-on-*n* technology MCT two-dimensional photodiode arrays in the MWIR range with 20-μm and 10-μm pixel pitch and compare them to corresponding *n*-on-*p* devices.

FOCAL PLANE ARRAY TECHNOLOGY

The fabrication of MCT-based IR detectors starts with the production of cadmium zinc telluride (CdZnTe) substrates with extraordinary crystal quality and very low dislocation density. AIM's technology for HOT application MCT detector manufacturing is based on the liquid phase epitaxial (LPE) growth of MCT on lattice-matched in-house-grown CdZnTe substrates from a tellurium-rich melt, using the vertical dipping method.[12] At this moment, crystal boules grown by the vertical Bridgman method with a diameter of 120 mm are the state-of-the-art, which enables manufacturing large size substrates with a high reproducibility (see Fig. 1). The dislocation density as measured by the Nakagawa etch method is an important criterion for the assessment of the material quality of substrates. For the development of HOT devices, the etch pit density is kept below 5×10^4 cm^{-2}. Our growth method allows growing large MCT wafers with an at present fair homogeneity in layer thickness (±1 μm) as well as in composition (±0.3-μm cut-off wavelength) in the LWIR–VLWIR cut-off wavelength range and (±0.15-μm cut-off wavelength) in the MWIR across irregularly-shaped wafers with an area equivalent to typically 1.5 inch (c.3.8 cm) diameter.

In Fig. 2, the schematic cross-section of a photodiode in *p*-on-*n* polarity is shown. The manufacturing and processing steps comprise

- MCT epilayer growth on CdZnTe substrate including an *n*-type doping by Indium (In) in the MCT melt
- Definition of the detector elements by Arsenic (As)-implantation (*p*-type) into the common *n*-type, In-doped MCT epitaxial layer, which creates a *p*-type well in an *n*-type absorber body
- Activation of As via a high-temperature annealing step
- Finishing of the detector technology (passivation, metallization, contacts)
- Selection of a suitable read-out integrated circuit (ROIC) available at AIM
- Hybridization of MCT detector chip and ROIC by a flip-chip bonding technology

Fig. 1. CdZnTe substrate on a 6″ (c.15-cm) Si wafer before polishing and a one Euro coin for size comparison. The wafer's dimension is 65 cm^2.

In *p*-on-*n* technology, the dark current of MCT detectors is in general limited at higher detector operating temperatures by the thermal diffusion current from the equilibrium *n*-MCT absorber region. The total carrier lifetime τ is given by[5]

$$\frac{1}{\tau} = \frac{1}{\tau_A} + \frac{1}{\tau_{SR}} + \frac{1}{\tau_{rad}} \quad (1)$$

with the Auger recombination lifetime τ_A, the Shockley–Read (SR) recombination lifetime τ_{SR}, and the radiative recombination lifetime τ_{rad}.

Due to proper processing, the number of metal vacancies in the MCT-layer is minimized, which drastically increases the SR lifetime. The diffusion current should then be limited by the Auger 1 recombination process in the *n*-MCT region, with radiative lifetimes large enough in properly designed devices.[5] With Auger 1 recombination, a minority carrier hole in the *n*-MCT absorbing layer recombines with an electron generating a hot electron in the conduction band for energy and momentum conservation.

RESULTS AND DISCUSSION

To measure the dark current and the electro-optical characteristics, the detector arrays have been hybridized either with ROIC chips or with a

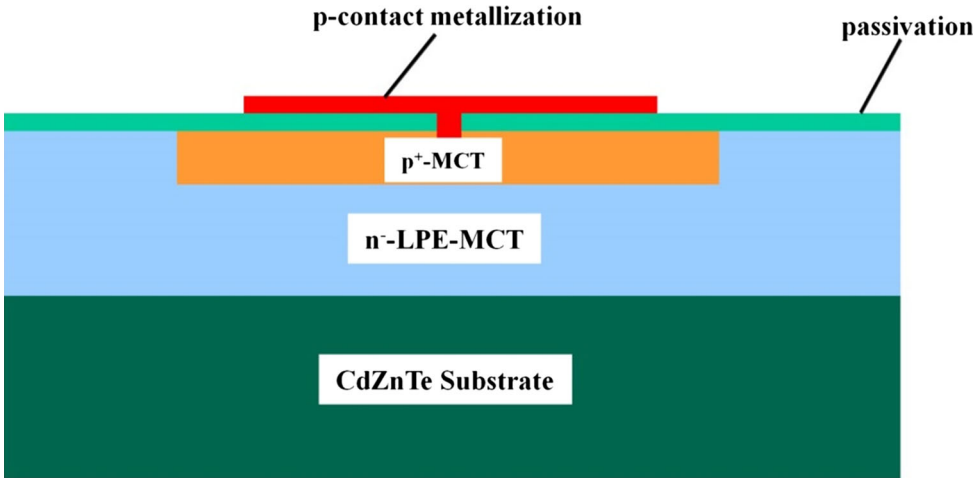

Fig. 2. Schematic cross-section of an MCT homo-junction photodiode detection layer in AIM's *p*-on-*n* planar photodiode technology.

fan-out circuit, which we will simply refer to subsequently as "fan-out". This fan-out contains structures to bias several photodiodes in parallel and to measure the overall current generated in these diodes. The shape of the simultaneously biased diode fields is that of a square and the size of these fields is given by the number of pixels along the edges. Additionally, guard structures are used, which consist of rows of diodes along the outer perimeter of the diode matrix. By adequately biasing those guard structures, the dark current contribution generated outside the pixel field is drained off. The dark currents are measured in a custom-made cryostat, where the temperature can be varied and set between 80 K and 300 K.

If not measured as fan-out in a cryostat, the FPA with ROIC chips are integrated in a detector dewar cooler assembly, which allows an electro-optical characterization at different operating temperatures ranging from 30 K to 220 K. The LWIR and MWIR FPA with a 20-μm pitch were integrated with an F/# 2.1 cold-shield configuration, the FPA with 10-μm pitch with an F/# 2.2 configuration.

LWIR 320 × 512, 20-μm Pitch

Low dark current LPE-MCT FPAs in *p*-on-*n* planar photodiode technology for detector operation in the 30–150 K temperature range were initially developed by AIM for the LWIR and VLWIR spectral ranges to serve both lower photon flux space environments as well as higher flux tactical applications. Dark currents around and below Tennant's 'Rule07'[13] were demonstrated on 320 × 512 pixel FPAs at a 20-μm pitch along with overall detection efficiencies (detected photoelectrons over photons incident onto the FPA) ≥60% in both *p*-on-*n* as well as *n*-on-*p* technology.[14] This implies that, for the same dark current performance, LWIR/VLWIR FPAs can now be operated at about 20-K higher temperature than with previous AIM technology.[15]

The thermal sensitivity of a detector characterizes both its detection efficiency as well as its noise behavior, to which the dark current also contributes. For NETD characterization, an approximate half-well integration capacitance filling level was set with the detector exposed to a 25°C large area blackbody scene (the ROIC full-well capacitance accounts for about 12.3 Me^-). The optical detection bandwidth ranges from about a 3-μm wavelength (given by the dewar window cut-on) to the detector QE cut-off wavelength, which is 11.0 μm at an 80-K temperature. The F/# of the cold shield is 2.1.

In order to quantify the detector operability, the common criterion that a pixel is regarded as defective if its NETD is above twice the median NETD or lower than half the median NETD is adopted here, though defect criteria as well as the defect limits are usually application-specific.

Figure 3 shows the measured NETD versus detector operating temperature for a *p*-on-*n* FPA (filled circles) and an *n*-on-*p* FPA (open circles) to the axis on the left and the corresponding NETD operability (filled and open square symbols) to the axis on the right.

For the *p*-on-*n* device, the NETD stays below 30 mK up to 110 K with the cut-off wavelength at about 10.2 μm in this case. Without discarding any pixels, at an 80-K operating temperature and an 11.0-μm QE cut-off, 0.45% of all pixels are considered defective. At 100 K, the fraction of defective pixels is 2.0% at a 10.4-μm QE cut-off, and at 110 K it is 3.2% at a 10.2-μm QE cut-off. Due to the increased symmetry in the NETD spread at lower temperatures such as at 50 K, we obtain only 0.20% defects at an 11.9-μm QE cut-off, and at 30 K, 0.12% of the pixels are considered defective at a corresponding 12.6-μm cut-off. It should be noted that the

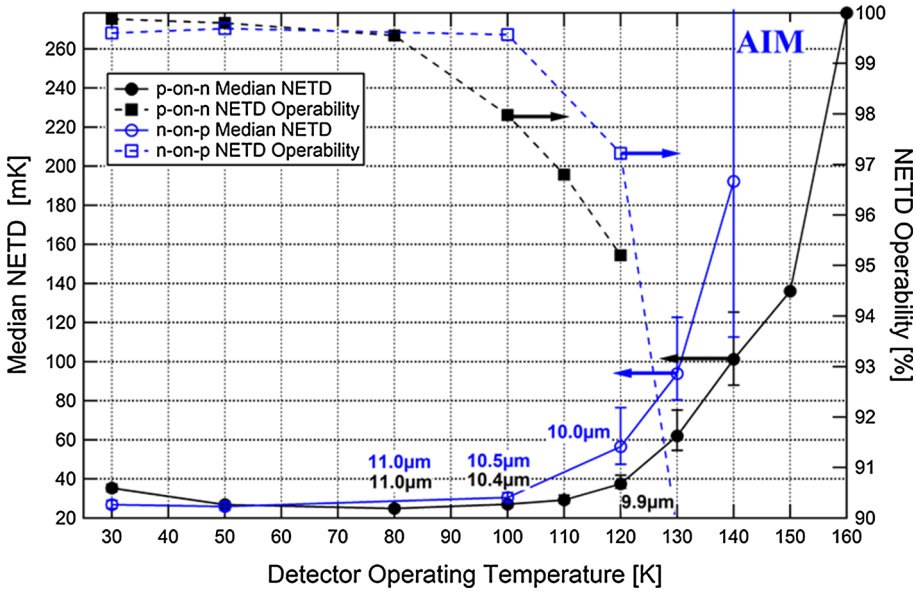

Fig. 3. Median NETD at about half-well IC filling level (left axis) and NETD operability (right axis) for two AIM *p*-on-*n* and *n*-on-*p* LWIR-MCT FPAs. An NETD below 30 mK is attained for operating temperatures up to 110 K (*p*-on-*n*, 10.2-μm cut-off) and 100 K (*n*-on-*p*, 10.5-μm cut-off). Numbers next to the data points indicate the cut-off wavelengths.

stated defect number takes several macro-defects into account which we expect to be able to rid of.

For the *n*-on-*p* device, at 100 K, a median NETD of 30.5 mK is achieved at a 10.5-μm cut-off wavelength. With the same NETD defect criterion as described before, and without discarding any pixels, at a 100-K operating temperature and a 10.5-μm QE cut-off, 0.43% of all pixels are considered defective. At 120 K and a 10.0-μm cut-off, the fraction of defective pixels is 2.8%. Again, it should be noted that the stated defect number takes several macro-defects into account which we expect to avoid in the future.

It should be noted that the demonstrated NETD and NETD operability depend significantly on the detector material quality, in particular for higher temperature operation. In this respect, the technology comparison made here is therefore illustrative at this point. The seemingly better operability of the *n*-on-*p* versus *p*-on-*n* approach is merely a statistical effect originating from the larger NETD distribution width with *n*-on-*p*.

MWIR 640 × 512, 20-μm Pitch

Recently, AIM has been successful in optimizing its MCT *n*-on-*p* planar detector technology for HOT applications while preserving high e/o-performance by improving the passivation process and introducing extrinsic *p*-doping with Au.[2,17] However, to realize ultra-compact IR-engines with optimized SWaP characteristics, a further increase in the FPA operating temperature to ≥160 K is required. The potential for a further increase in operating temperature in the current MWIR *n*-on-*p* planar technology seems to be limited, for example, by the capability to provide low *p*-type doping levels $<5 \times 10^{15}$ cm^{-3} with high reproducibility. Encouraged by the outstanding results for *p*-on-*n* VLWIR FPAs, this approach has been applied to MWIR detector arrays. Initially, MCT MWIR FPAs were realized in a 20-μm pitch design (640 × 512 pixel format) and tested in an F/# 2.1 configuration. Table I shows an overview of MCT MWIR detector technologies at AIM including our HOT device generations based on *n*-on-*p* technology and the recently developed *p*-on-*n* approach.

In Fig. 4, the mean NETD is plotted as a function of operating temperature (T_{op}) for three FPAs manufactured using different *n*-on-*p* detector technologies (see Table I) together with one FPA from recent *p*-on-*n* technology. The MCT epitaxial layer of this array is extrinsically *n*-doped with In during growth (*n*-doping of about 3×10^{15} cm^{-3}). The NETD has been measured under half-well filling level condition at 27°C blackbody scene and the integration time has been adjusted for each T_{op} to compensate for the cut-off shift to shorter wavelengths with increasing operating temperature. (The full-well capacitance of the ROIC accounts for about 3.3 Me$^-$.) The cut-off wavelength of all FPAs is in the range of 5.2 μm ± 0.1 μm at 80 K. The background-limited performance (BLIP) condition is roughly indicated by the dashed line and serves as a guide for how much the NETD has increased by the rising impact of the dark current. The *p*-on-*n* FPA performs better than the 'optimized standard' and HOT Gen1 FPA approaches and shows comparable performance to the HOT GEN2 FPA. The NETD stays close to BLIP for operating temperatures up to 150 K in both cases. At 160 K, a still good NETD of ~24 mK is derived for the *p*-on-*n* FPA. Even at

Table I. Overview of MCT MWIR detector technologies at AIM including HOT device generations and the recent *p*-on-*n* approach[17]

Detector technology	Characteristics	Operating temperature
Standard	*n*-on-*p*; vacancy doping	80 K typical
Optimized standard	*n*-on-*p*; vacancy doping; improved homogeneity; substrate quality etc.	95 K typical, up to 120 K
HOT GEN1	*n*-on-*p*; extrinsic *p*-doping with Au (high concentration); standard passivation process	120 K typical, up to 140 K
HOT GEN2	*n*-on-*p*; extrinsic *p*-doping with Au (low concentration); optimized passivation process	140 K typical, up to 160 K
p-on-*n*	In and As doping	Comparable to HOT GEN2

170 K, the NETD stays with 27 mK below 30 mK, which is a limit for certain imaging applications. At 180 K, the impact of the dark current is obvious, which results in an NETD value slightly above 40 mK and a reduced integration time.

The operability of the FPA, plotted in Fig. 5 as a function of T_{op}, is excellent and better than 99.8% up to 160 K and still good at 170 K with 99.5%. The criteria for defective pixels are included in the figure caption.

Higher-temperature detector operation is limited on the one hand by the MCT thermal dark current which fills the integration capacitance with unwanted electrical charges limiting the dynamic detector range and on the other hand by the white noise associated with the dark current. Another limit constitutes the non-white noise contributions from "blinking" pixels ("random telegraph signal" or RTS noise) which suddenly show a temporary change in video output signal. In particular, low-frequency noise pixels lead to an asymmetric broadening of the noise and therefore NETD distributions towards larger values and must eventually be categorized as defective, depending on the precise detector operating parameters such as frame rate and number of averaged frames. The frequency spectrum and the fraction of blinking pixels within a given bandwidth is in general also dependent on the operating temperature and may also be dependent on the illumination conditions.

For the characterization of the non-white noise behavior, we consider the knee frequency or corner frequency f_0, which we define as the frequency at which the power spectral density is twice the white noise level. The measurements were carried out in the dark field in order not to be affected by photonic background-generated artifacts; for example, by blackbody illumination-induced fixed pattern noise. This way, the bare detector physics is characterized. However, under these conservative conditions, the comparatively large white noise level from illumination is absent which would likely obscure a significant number of the RTS pixels observed here.

For analysis, a number of 256 × 256 pixel subframes was continuously recorded, yielding a 0.15-Hz to 300-Hz detection bandwidth. This means that blinking pixels leading to a broadening of the $1/f^k$ tail in the noise power spectrum in that frequency range could be detected. For data evaluation, an algorithmic approach based on Ref. 16 was used. The restriction to a sub-frame analysis originated from hardware constraints.

Knee frequencies are spatially distributed over the considered range of interest (ROI) in a random fashion, as may be discerned from Fig. 6 for the case of a high 140-K detector operating temperature and a 5.0-μm cut-off wavelength. The cumulative histograms of the knee frequency distributions within the measurement bandwidth at temperatures between 90 K and 160 K are shown in Fig. 7. At a 90-K temperature, more than 99% of all pixels have

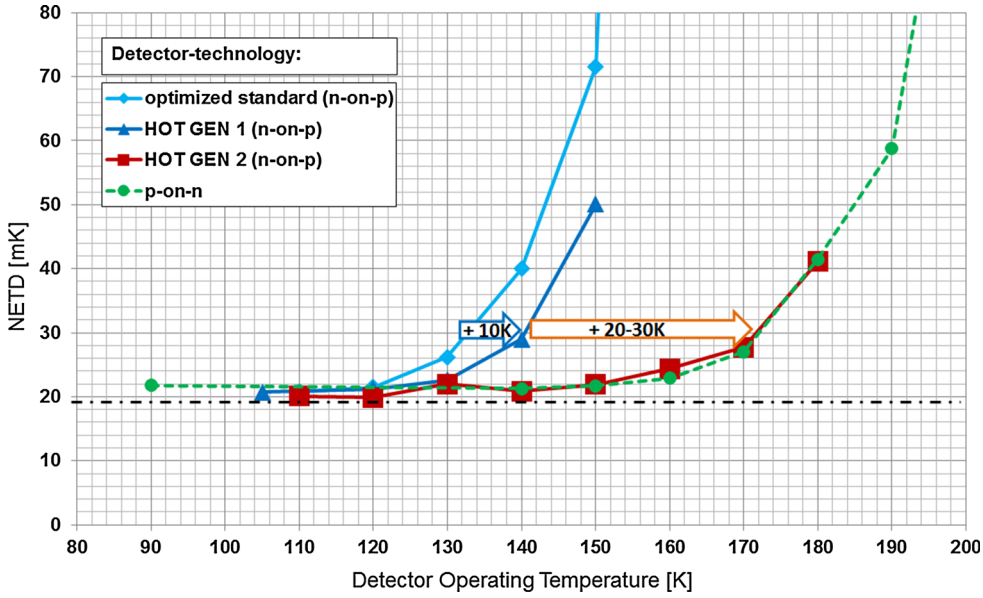

Fig. 4. NETD as a function of the operating temperature for FPAs made from three different *n*-on-*p* and recently introduced *p*-on-*n* detector technologies (using data from Ref. 17). The dashed line indicates BLIP. The results of the *p*-on-*n* technology are comparable to the HOT GEN2 *n*-on-*p* technology.

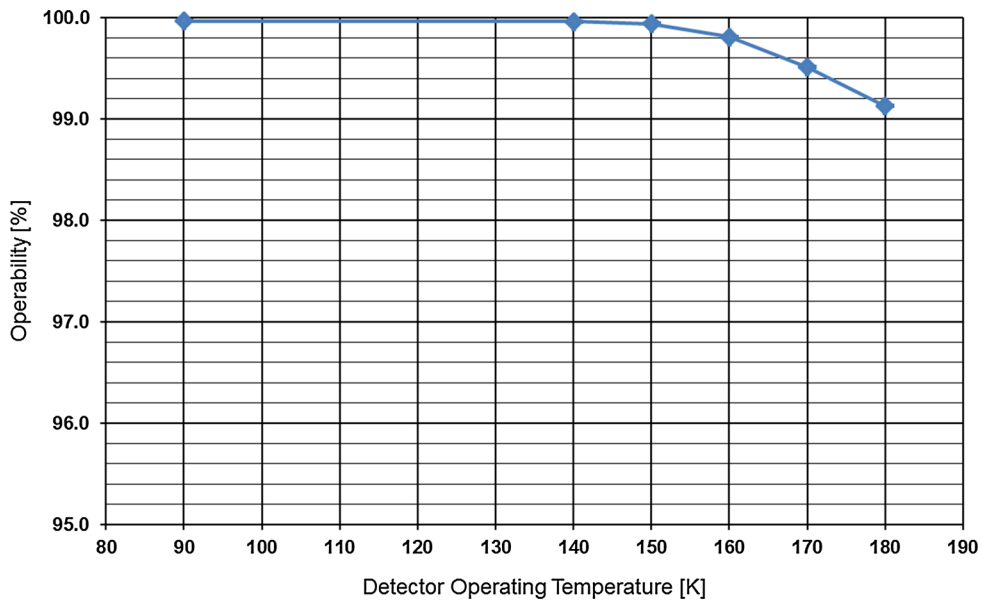

Fig. 5. Operability as a function of FPA operating temperature of an AIM *p*-on-*n* MWIR detector [640 × 512, 20-μm pitch, F/2.05; defect pixel criterion: (0,2) × NETD mean, (0.5,2) × gain mean, (0,5) × noise median].

knee frequencies below the resolution limit of about 0.15 Hz. At 160 K, this fraction is still above 93%.

For a typical application with a 100-Hz frame rate and recording 35 frames for averaging, the upper and lower band limits are indicated by the red vertical lines in the graph, and the expected fraction of blinking pixels is a few percent at the highest set operating temperatures in the dark field under worst case observation conditions. As expected, the fraction of blinking pixels increases in general with temperature (activation energy).

To demonstrate the high performance and image quality of the 640 × 512 pixel, 20-μm pitch *p*-on-*n* MCT detector array, IR images of a person are shown in Fig. 8. The images were taken with an F/# 1.5, f = 28 mm optics. Only a basic 2-point non-uniformity correction (NUC) and a standard bad pixel replacement (BPR) were applied. For operating temperatures between 120 K and 180 K, fine structures such as single hairs of the head or of the eyelids and thermal structures of the skin can be clearly resolved, which proves the high thermal and

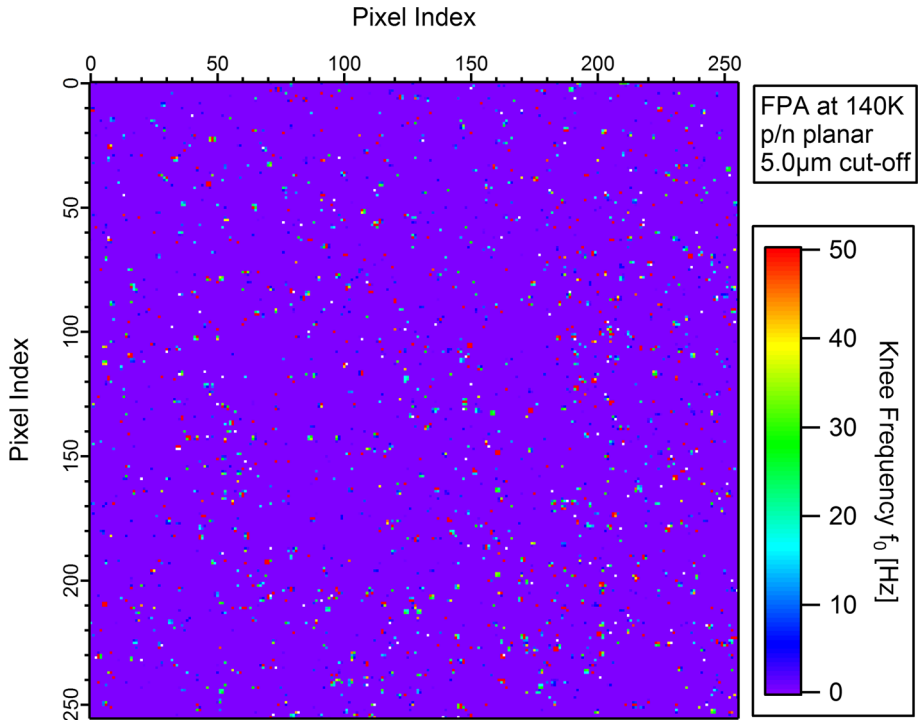

Fig. 6. Spatial distribution of knee frequencies over a 256 × 256 pixel ROI in a 0.15- to 300-Hz bandwidth for a *p*-on-*n* planar technology MCT LWIR FPA at 140 K. The spatial distribution of elevated knee frequencies appears to be random on the considered scale.

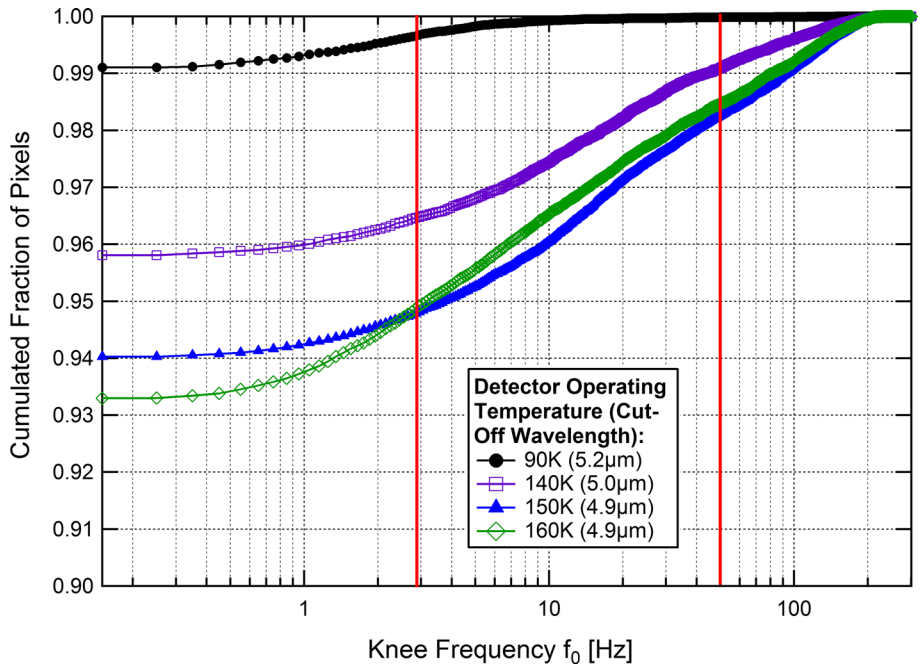

Fig. 7. Cumulative histograms of the knee frequency distributions within a 0.15- to 300-Hz bandwidth for an MWIR MCT FPA at operating temperatures between 90 K and 160 K and facing a dark field. Numbers in parentheses indicate the cut-off wavelengths at the given detector temperatures.

spatial resolution. At an operating temperature of 200 K, the contribution of the dark current is apparent, and at an operating temperature of 220 K, the noise in the image increases considerably, but the thermal contrast still stays good enough to clearly resolve the person.

Fig. 8. Infrared images taken with an AIM p-on-n MWIR MCT FPA 640 × 512 and 20-μm pitch of a person for detector operating temperatures between 120 K and 220 K. Only 2-point NUC and bad pixel replacement has been applied. The detector's cut-off wavelength is 5.25 μm at 80 K.

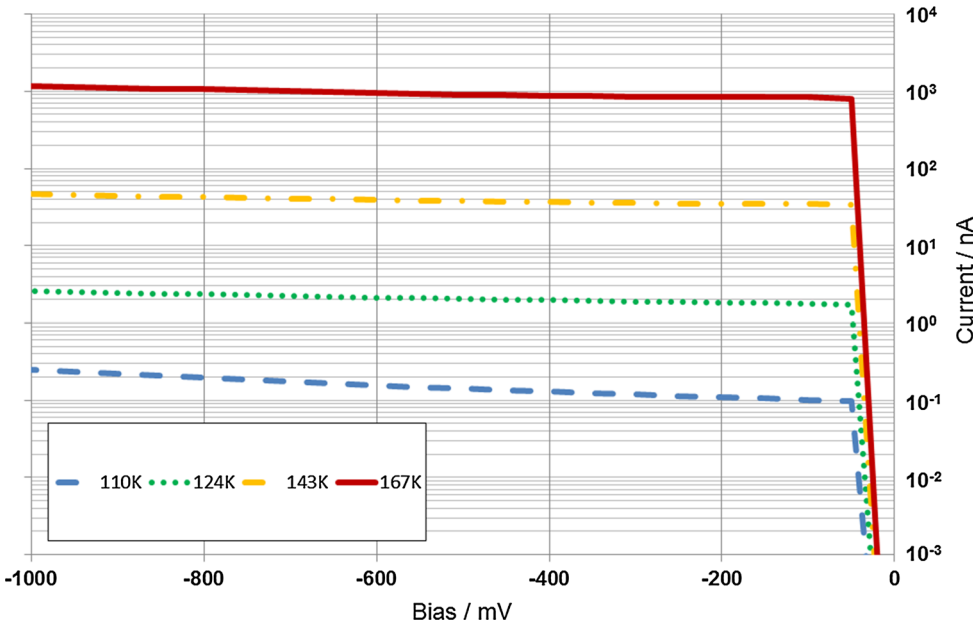

Fig. 9. Dark current as a function of detector bias voltage of a 100 × 100 *p*-on-*n* planar photodiode pixel array with a 10-μm pixel pitch for different operating temperatures; applied guard-bias: −250 mV (cut-off wavelength: 5.20 μm at 80 K).

MWIR 1024 × 768, 10-μm Pitch

AIM started the development of a 10-μm pixel pitch MCT detector technology in 2013 and had realized first FPAs in XGA format by the end of 2015. The MCT epilayers were grown with LPE and further processed in *n*-on-*p* technology using extrinsic *p*-doping with Au. This technology allows for elevated operating temperatures in the range of ~140 K.[17] For a further increase in the operating temperature, the *p*-on-*n* technology developed with 20-μm pitch detectors has been adapted for 10-μm pitch detector arrays.

In Fig. 9, the dark current–voltage (I-V) characteristics of a 100 × 100 pixel *p*-on-*n* planar photodiode array with a 10-μm pixel pitch at different temperatures between 100 K and 167 K are shown. The measurements were done with a fan-out structure. The results show that the current level stays almost flat across a wide bias range up to −1000 mV for each chosen temperature between 110 K and 164 K. This feature is helpful for an improved operability and is necessary if the application demands higher bias levels for detector stability.

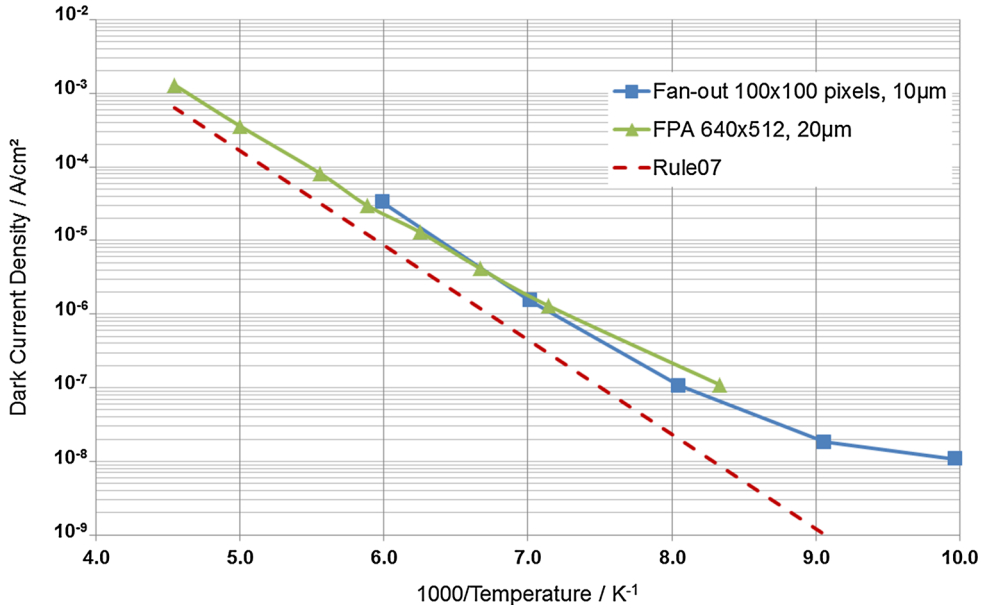

Fig. 10. Dark current density (blue boxes) of a 100 × 100 pixel subarray of a 10-μm pitch detector, measured with a fan-out structure compared with the corresponding values of the *p*-on-*n* FPA with 640 × 512 pixels and 20-μm pitch. The dark current density as represented by the red dashed line is calculated according to the Rule07 first published by Tennant et al.[13] (Color figure online).

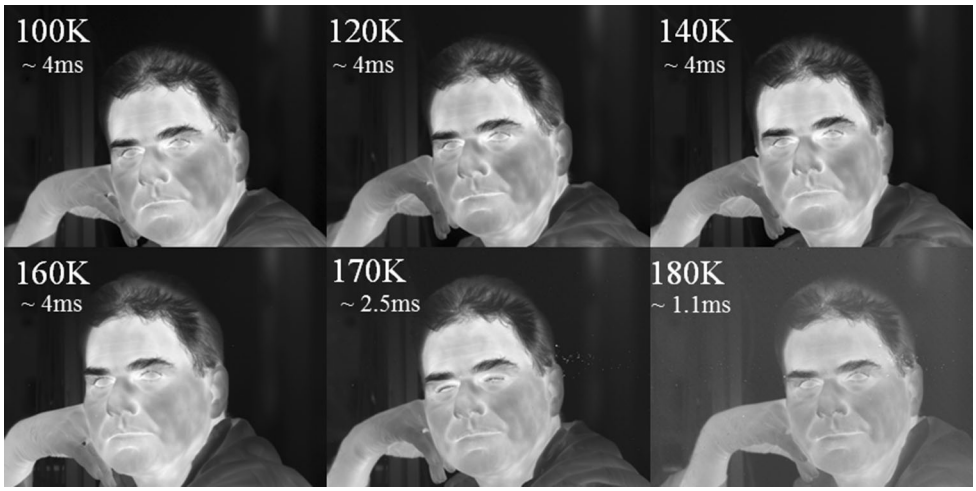

Fig. 11. Infrared images taken with an AIM *p*-on-*n* MWIR MCT FPA 1024 × 768 and 10-μm pitch of a person for detector operating temperatures between 100 K and 180 K. Only 2-point NUC and BPR has been applied. The detector's cut-off wavelength is 5.20 μm at 80 K. The full-well capacitance of the ROIC accounts for about 5.5 Me^- for integrate then read readout mode.

In Fig. 10, the dark current density of a 100 × 100 pixel subarray of a *p*-on-*n* detector with a 10-μm pitch is shown along with the data of the 20-μm pitch MWIR detector discussed in the previous section and compared to the Rule07 as published by Tennant.[13] At higher temperatures, the dark current data follow Rule07 in an almost parallel fashion. The absolute current values are by a factor of ~3 higher than predicted by Rule07. This is in line with the statement of Lee et al.[18] that the Rule 07 is modeled to an Auger1-limited *p*-on-*n* detector with an absorber *n*-type doping level of 1×10^{15} cm^{-3}, because, in the Auger1 limit, the dark current scales with the majority carrier density. A further decrease in dark current might be achieved by a further lowering of the absorber *n*-type doping level.

As a demonstration of the high performance and image quality of the 1024 × 768, 10-μm pitch detector array, IR images of a person are shown in Fig. 11. The images were taken with an F/# 1.5, f = 28 mm optics. Only a basic 2-point non-uniformity correction (NUC) and a standard BPR were applied. Fine structures such as single hairs of the head and the eyebrows as well as thermal structures of the skin can be clearly resolved at all shown

temperatures. From 170 K, the impact of dark current rises significantly, but the thermal contrast is still high enough for good resolution of the person. This is also underlined by the decrease of integration time, which stay nearly constant from 100 K to 160 K at about 4 ms and diminishes at 170 K to 2.5 ms and 1.1 ms at 180 K.

CONCLUSION

Driven by the growing market need for low dark current MWIR and LWIR MCT FPAs for higher operating temperature field applications, AIM has first developed specific manufacturing processes and subsequently manufactured and characterized MCT detector arrays in both *n*-on-*p* as well as *p*-on-*n* planar photodiode technologies.

Dark currents have been significantly reduced for LWIR FPA with a cutoff wavelength of 11 μm (at 80 K) in both polarities. For the *p*-on-*n* detector version, thermal resolution NETD stays below 30 mK for operating temperatures up to 110 K. This allows for the same dark current performance at a 20- to 30-K higher operating temperature than with previous AIM technology.

In the MWIR, the *p*-on-*n* technology, demonstrated for a 640 $\times$ 512 pixel FPA with 20-μm pixel pitch provides comparable results as the most advanced *n*-on-*p* HOT technology. NETD values better than 30 mK have been obtained up to 170 K. In addition, the *p*-on-*n* MWIR FPA shows a full random spatial distribution of knee frequencies in a detection bandwidth between 0.15 Hz and 300 Hz in the dark field for different operating temperatures.

MWIR FPA have been realized with 1024 $\times$ 768 pixels and a small 10-μm pixel pitch in *p*-on-*n* technology, demonstrating high detector performance up to 160 K.

ACKNOWLEDGEMENTS

The presented work has partially been supported by the European Space Agency (ESA) under ESTEC contract 4000107414/13/NL/SFe and by the German Ministry of Defense. We gratefully acknowledge this support.

REFERENCES

1. R. Wollrab, A. Bauer, H. Bitterlich, M. Bruder, S. Hanna, H. Lutz, K.-M. Mahlein, T. Schallenberg, and J. Ziegler, *J. Electron. Mater.* 40, 1618 (2011). doi:10.1007/s11664-011-1659-0.
2. H. Lutz, R. Breiter, H. Figgemeier, T. Schallenberg, W. Schirmacher, and R. Wollrab, in *Proceedings of SPIE Conference*, vol. 9070 (2014), p. 90701D. doi: 10.1117/12.2050427.
3. A. Rogalski, *Prog. Quant. Electron.* 36, 342 (2012). doi: 10.1016/j.pquantelec.2012.07.001.
4. A. Rogalski, P. Martyniuk, and M. Kopytko, *Rep. Prog. Phys.* 79, 046501 (2016). doi:10.1088/0034-4885/79/4/046501.
5. M.A. Kinch, Fundamentals of infrared detector materials. (SPIE Press, Bellingham/WA, 2007), ISBN 97808194 67317.
6. M.A. Kinch, State-of-the-art infrared detector technology. (SPIE Press, Bellingham/WA, 2014), ISBN 9781628412895.
7. L. Pillans, I. Baker, and R.K. McEwen, in *Proceedings of SPIE Conference*, vol. 9070 (2014), p. 90701E. doi: 10.1117/12.2050327.
8. Y. Karni, P. Klipstein, E. Avnon, E. Berkowitz, O. Cohen, Y. Cohen, R. Dobromislin, I. Hirsh, O. Klin, I. Lukomsky, I. Pivnik, O. Rozenberg, I. Shtrichman, M. Singer, S. Sulimani, and E. Weiss, in *Proceedings of SPIE Conference*, vol. 9070 (2014), p. 90701F. doi: 10.1117/12.2049691.
9. Y. Reibel, R. Taalat, A. Brunner, L. Rubaldo, A. Augey, A. Kerlain, N. Péré-Laperne, A. Manissadjian, O. Gravrand, P. Castelein, and G. Destéfanis, in *Proceedings of SPIE Conference*, vol. 9451 (2015), p. 945110. doi:10.1117/12.2179212.
10. D. Ramirez, E. Plis, S. Myers, C. Morath, V. Cowan, and S. Krishna, in *Proceedings of SPIE Conference*, vol. 9451 (2015), p. 945113. doi: 10.1117/12.2176908.
11. Y. Reibel, N. Péré-Laperne, L. Rubaldo, T. Augey, G. Decaens, V. Badet, L. Baud, J. Roumegoux, A. Kessler, P. Maillart, N. Ricard, O. Pacaud, and G. Destéfanis, in *Proceedings of SPIE Conference*, vol. 9451 (2015), p. 94512E. doi:10.1117/12.2178954.
12. M. Bruder, H. Figgemeier, L. Palm, J. Ziegler, and H. Maier, in *Proceedings of SPIE Conference*, vol. 2554 (1995), p. 137. doi: 10.1117/12.218181.
13. W.E. Tennant, D. Lee, M. Zandian, E. Piquette, and M. Carmody, *J. Electron. Mater.* 37, 1406 (2008). doi: 10.1007/s11664-008-0426-3.
14. S. Hanna, D. Eich, K.-M. Mahlein, W. Fick, W. Schirmacher, R. Thöt, J. Wendler, and H. Figgemeier, *J. Electron. Mater.* 45, 4542 (2016). doi:10.1007/s11664-016-4523-4.
15. H. Lutz, R. Breiter, D. Eich, I. Rühlich, S. Rutzinger, T. Schallenberg, J. Wendler, R. Wollrab, and J. Ziegler, in *Proceedings of SPIE Conference*, vol. 8185 (2011), p. 818504. doi: 10.1117/12.900347.
16. V. Goiffon, G.R. Hopkinson, P. Magnan, F. Bernard, G. Rolland, and O. Saint-Pe, *IEEE Trans. Nucl. Sci.* 56, 2132 (1999). doi:10.1109/TNS.2009.2014759.
17. H. Lutz, R. Breiter, D. Eich, H. Figgemeier, P. Fries, S. Rutzinger, and J. Wendler, in *Proceedings of SPIE Conference*, vol. 9819 (2016), p. 91891Y. doi: 10.1117/12.2223841.
18. D. Lee, M. Carmody, E. Piquette, P. Dreiske, A. Chen, A. Yulius, D. Edwall, S. Bhargava, M. Zandian, and W.E. Tennant, *J. Electron. Mater.* 45, 4587 (2016). doi: 10.1007/s11664-016-4566-6.